Diffusion lengths of silicon solar cells from luminescence images

P. Würfel,[a] T. Trupke,[b] and T. Puzzer
Centre of Excellence for Advanced Silicon Photovoltaics and Photonics, University of New South Wales, Sydney, NSW 2052, Australia

E. Schäffer, W. Warta, and S. W. Glunz
Fraunhofer Institut für Solare Energiesysteme, Heidenhofstrasse 2, Freiburg 79110, Germany

(Received 2 May 2007; accepted 8 May 2007; published online 27 June 2007)

A method for spatially resolved measurement of the minority carrier diffusion length in silicon wafers and in silicon solar cells is introduced. The method, which is based on measuring the ratio of two luminescence images taken with two different spectral filters, is applicable, in principle, to both photoluminescence and electroluminescence measurements and is demonstrated experimentally by electroluminescence measurements on a multicrystalline silicon solar cell. Good agreement is observed with the diffusion length distribution obtained from a spectrally resolved light beam induced current map. In contrast to the determination of diffusion lengths from one single luminescence image, the method proposed here gives absolute values of the diffusion length and, in comparison, it is much less sensitive to lateral voltage variations across the cell area as caused by local variations of the series resistance. It is also shown that measuring the ratio of two luminescence images allows distinguishing shunts or surface defects from bulk defects. © *2007 American Institute of Physics*. [DOI: 10.1063/1.2749201]

INTRODUCTION

Current methods for determining spatial variations of the diffusion length include spectral response or spectrally resolved light beam induced current[1] (LBIC) and electroluminescence imaging.[2] Spatially resolved spectral LBIC is a mapping system and, while very accurate, it is relatively slow. A scan on an industrial sized solar cell (e.g., 10×10 cm^2) with 200×200 pixels takes several hours. Electroluminescence imaging has been proposed by Fuyuki *et al.* as a much faster alternative technique.[2,3] Typical data acquisition times for electroluminescence images taken with a silicon charge coupled device (CCD) camera with 1024×1024 pixels are on the order of only 1 s.[4–6] However, the approach proposed by Fuyuki *et al.* of using a single electroluminescence image as a reliable and quantitative measurement of the diffusion length can be highly inaccurate for various reasons that will be discussed in this paper.

The determination of the diffusion length from spectral response or from spectrally resolved LBIC is based on the fact that the contribution to the measured photocurrent of electron-hole pairs generated at variable distance from the *p-n* junction depends on the minority carrier diffusion length. Carriers do not effectively contribute to the photocurrent if the penetration depth of the incident photons is much larger than the diffusion length. In a different method for the determination of the diffusion length to be discussed here, this situation is reversed. It measures luminescence signals and is based on the fact that photons generated inside the bulk of a solar cell at a point further away from the surface than their own penetration depth will be reabsorbed before reaching the surface and will therefore not contribute to the measured emission intensity. The rate of spontaneous emission of crystalline silicon at room temperature and thus the emitted luminescence intensity is considerable in the wavelength range from 850 to 1250 nm, corresponding to photon penetration depths ranging from 20 μm to several centimeters, i.e., from much smaller than the thickness of a silicon solar cell (typically 200–300 μm) to much larger than that thickness. Restricting the measured luminescence signal to specific wavelength ranges by using suitable filters, thus, allows information to be gained about either the total carrier density across the entire sample thickness (long wavelength luminescence with long penetration depth) or about the carrier density near the front surface (short wavelength luminescence with short penetration depth). The knowledge about the total carrier density and about the carrier density near the front, respectively, allows the carrier density profile and, thereby, the diffusion length to be determined, as will be shown theoretically and experimentally below.

Importantly, this method can, in principle, either be applied to photoluminescence (PL) imaging[7] measurements on silicon wafers at an early stage of solar cell fabrication or to electroluminescence (EL) measurements carried out on fully processed solar cells. It may also be applied to other materials suited for solar cell fabrication.

THEORY

The quantitative description of the dependence of the emission spectrum on the minority carrier diffusion length is carried out in two steps. Firstly, we describe analytically how the diffusion length affects the depth distribution of minority carriers that are injected into the base of a solar cell via an applied voltage. In a second step, we then describe how that minority carrier distribution affects the emission spectrum.

[a]On leave from University of Karlsruhe.
[b]Electronic mail: thorsten@trupke.de

The resulting relationship between the diffusion length and the emission spectrum is then used to derive a quantitative relationship between the diffusion length and the *ratio* of luminescence signals in two different spectral ranges. These spectral ranges are specified experimentally by the transmission of filters being used for the two luminescence measurements.

Carrier distribution

We consider the injection of electrons from the *p*-*n* junction into the *p*-type base of a solar cell. With an applied voltage V_{appl}, the electron concentration $n_e(0)$ on the *p* side of an abrupt *p*-*n* junction that is located at $x=0$ is given as

$$n_e(0) = \frac{n_i^2}{N_A} \exp\left(\frac{eV_{\mathrm{appl}}}{kT}\right), \tag{1}$$

where n_i is the intrinsic carrier concentration and N_A is the doping concentration in the base. The rear surface at $x=d$ is characterized by a surface recombination velocity S such that the electron diffusion current at the rear $j_e(d)$ is given by

$$j_e(d) = -D_e \frac{dn_e}{dx}(d) = Sn_e(d), \tag{2}$$

with D_e the electron diffusion coefficient. Note that $j_e(d)$ in Eq. (2) is a particle current, not an electrical current.

With these two boundary conditions, the electron distribution $n_e(x)$ follows from the continuity equation for electrons in steady state,

$$\frac{d^2n_e}{dx^2} - \frac{n_e}{L_e^2} = 0, \tag{3}$$

and is

$$n_e(x) = A \exp\left(\frac{x}{L_e}\right) + B \exp\left(-\frac{x}{L_e}\right), \tag{4}$$

with

$$A = n_e(0)\frac{1-r}{1-r+(1+r)\exp(2d/L_e)} \tag{5}$$

and

$$B = n_e(0)\frac{1+r}{1+r+(1-r)\exp(-2d/L_e)},$$

where $L_e=\sqrt{D_e\tau_e}$ is the diffusion length and $r=SL_e/D_e$.

Equations (1)–(5) allow the calculation of the minority carrier density profile as a function of the applied voltage, of the diffusion length, and of the rear surface recombination velocity.

Photon emission

Photons with energy $\hbar\omega$ in the energy interval $d\hbar\omega$ are generated by spontaneous radiative recombination of electrons and holes at a rate $g_\gamma(x,\hbar\omega)$ per energy. For nondegenerate electron and hole concentrations, the generation rate of photons by radiative recombination via band-band transitions is given by[8,9]

$$g_\gamma(x,\hbar\omega) = \alpha(\hbar\omega)\frac{(\hbar\omega)^2}{4\pi^2\hbar^3c^2}\frac{1}{\exp\{[\hbar\omega-\Delta\eta(x)]/kT\}-1}, \tag{6}$$

where $\alpha(\hbar\omega)$ is the absorption coefficient for band to band transitions and $\Delta\eta(x)$ is the local separation of the quasi-Fermi-energies. In most practical cases, the -1 in the denominator of Eq. (6) can be neglected. Under the assumption of low injection conditions within the base, Eq. (6) can then be rewritten as

$$g_\gamma(x,\hbar\omega) = \alpha(\hbar\omega)\frac{(\hbar\omega)^2}{4\pi^2\hbar^3c^2}\exp\left(\frac{-\hbar\omega}{kT}\right)\left[\frac{n_e(x)N_A}{n_i^2}\right]. \tag{7}$$

Equation (7) predicts the local spectral distribution of spontaneously emitted photons inside the sample. The same spectral distribution of photons would also be measured outside the sample if no reabsorption on the way to the surface occurred.

The emitted photon current $dj_{\gamma,em}(\hbar\omega)$ in the energy interval $d\hbar\omega$ that is measured outside the sample follows from integrating the contributions from the photon generation rate $g_\gamma(x,\hbar\omega)$ over the thickness of the solar cell. Accounting for reabsorption with absorption coefficient α and taking into account one reflection at the front (R_f) and one reflection at the rear (R_r) yields

$$\frac{dj_{\gamma,em}}{d(\hbar\omega)}(\hbar\omega) = [1-R_f(\hbar\omega)]\int_0^d (g_\gamma(x,\hbar\omega)\{\exp[-\alpha(\hbar\omega)x] + R_r(\hbar\omega)\exp[-\alpha(\hbar\omega)(2d-x)]\})dx \tag{8}$$

for the emitted photon current. Multiple reflections and, thereby, the influence of light trapping on the spectrum are neglected in Eq. (8), an assumption that is justified by the selection of short pass filters used in our experiments, as discussed below. In the above treatment, it is assumed that nonradiative recombination is the dominant recombination mechanism. The generation of electron-hole pairs by the reabsorption of spontaneously emitted photons (photon recycling) is therefore neglected in the continuity equation for the electrons in Eq. (3). By the same reasoning, photons emitted into directions where they are totally reflected are left out of the analysis, considering that their reabsorption will not give rise to newly emitted photons. If radiative recombination were dominant, as in many direct semiconductor materials, the electron concentration would become homogeneous through photon recycling and no information on the electron diffusion length could be gained from the shape of the emission spectrum.

With the electron distribution in Eq. (4), the emitted photon spectrum is found from Eqs. (7) and (8) by numerical integration. The resulting spectrum thus contains the information on the distribution of the electrons.

Detection of emitted photons

In previous work on luminescence imaging of silicon solar cells and silicon wafers, a silicon CCD camera has been used, providing excellent spatial resolution of 1024 $\times$ 1024 pixels. On the other hand, a silicon sensor is not

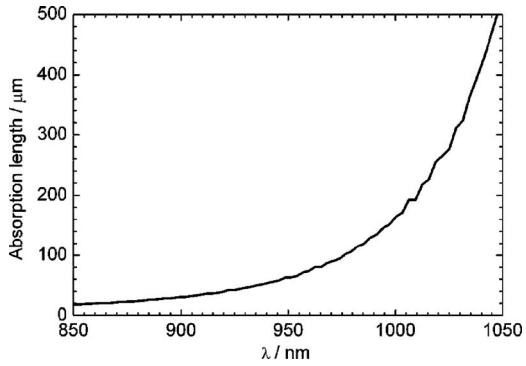

FIG. 1. (Color online) Absorption length of photons as a function of wavelength according to literature data for the absorption coefficient of crystalline silicon at room temperature (Ref. 10).

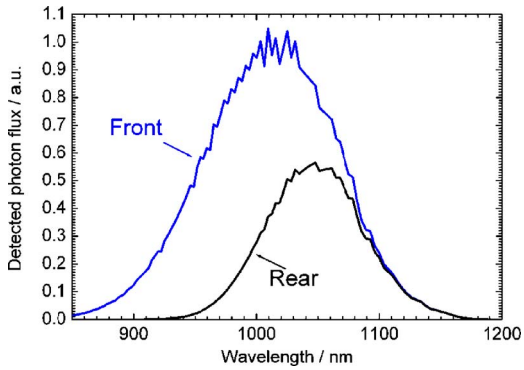

FIG. 2. (Color online) Calculated emission rate multiplied by the sensitivity of a silicon CCD detector without reabsorption (front) and with reabsorption on a 200 μm optical path (rear).

particularly sensitive to the long wavelength radiation emitted by silicon samples. Since long wavelength radiation is poorly absorbed, it may be scattered laterally within the CCD array and may eventually be absorbed in the wrong pixel, thereby causing a smearing of the contrast. In addition, long wavelength light is also subject to light trapping within the silicon sample itself, which can lead to long wavelength photons escaping the sample far away from the point where they were generated, an effect that also leads to a smearing of the contrast. Measurements with an InGaAs camera, which is strongly absorbing across the entire spectral range in which significant luminescence from silicon occurs (850–1250 nm), would avoid the contrast smearing within the CCD itself but would still be affected by light scattering within the measured sample. In fact, that latter effect would be even more pronounced than with a silicon CCD camera, because an InGaAs sensor measures the entire long wavelength tail of the luminescence, which is most strongly affected by light trapping and to which a silicon CCD camera is insensitive.

To reduce these problems, we restrict the detection of photons to wavelength $\lambda < \lambda_{\text{cutoff}}$ by using a short pass filter, which blocks photons that have a penetration depth larger than the thickness of the sample. This cutoff filter will eliminate all long wavelength emitted light, which is enhanced by light trapping in the solar cell, which also justifies the above approach of neglecting multiple reflections within the sample in the derivation of Eq. (8). The absorption length $1/\alpha$ of emitted photons as a function of the wavelength λ is shown for silicon at $T=300$ K in Fig. 1 using absorption coefficient data determined by Weakliem and Redfield.[10] This dependence suggests a cutoff wavelength for the short pass filter λ_{cutoff} between 1000 and 1050 nm. By using 1000 and 900 nm filters in the luminescence images presented in this study, the influence of lateral smearing within the sample is completely eliminated.

To properly model the intensity detected by the CCD camera, its sensitivity $\Phi_{\text{camera}}(\hbar\omega)$ (including the transmission of its lens) and the transmission of the short pass filter T_{filter} must be included

$$\frac{dj_{\gamma,\text{detect}}}{d(\hbar\omega)}(\hbar\omega) = T_{\text{filter}}(\hbar\omega)\Phi_{\text{camera}}(\hbar\omega)\frac{dj_{\gamma,\text{em}}}{d(\hbar\omega)}(\hbar\omega). \qquad (9)$$

Figure 2 shows the photon generation rate $g_\gamma(\hbar\omega)$ calculated according to Eq. (6) using the absorption coefficient data from Weakliem and Redfield[10] multiplied by $\Phi_{\text{camera}}(\hbar\omega)$. The peak of the rate of spontaneous emission itself (prior to multiplication by the sensitivity of the camera) is at $\lambda = 1140$ nm. However, the sensitivity of the camera decreases strongly with increasing wavelength, shifting the peak in the *detected* photon current to ~1020 nm. Numerical integration of the total and of the detectable photon currents, respectively, shows that, depending on the exact values for $\Phi_{\text{camera}}(\hbar\omega)$, only on the order of 5% of the total luminescence signal that is emitted by silicon solar cells can be captured with a silicon CCD camera, which suggests that a significant improvement in the sensitivity could be achieved by using, e.g., an InGaAs camera.

Influence of the diffusion length on the detected spectrum

Figure 2 demonstrates the principle of how the carrier distribution influences the emitted spectrum. The two curves represent the photon fluxes that would be detected by the CCD camera for the same carrier density located either near the front or at the rear surface of a 200 μm thick wafer. While no difference is observed at long wavelengths, the detected photon flux at shorter wavelength is strongly reduced for the emission from the rear surface due to reabsorption of photons on their way to the front surface. The ratio of the luminescence intensities at long and short wavelengths, respectively, thus contains information about the optical path the photons have traveled within the sample and, thereby, about the carrier distribution.

The spectral dependence of the detectable photon current for realistic carrier distributions was calculated according to Eqs. (7)–(9) for variable diffusion lengths. We assumed a solar cell with 300 μm thickness and an applied voltage of $V_{\text{appl}}=0.6$ V. Front and rear reflectances were assumed to be constant over the wavelength range considered. The resulting spectra were then multiplied with transmission curves of dif-

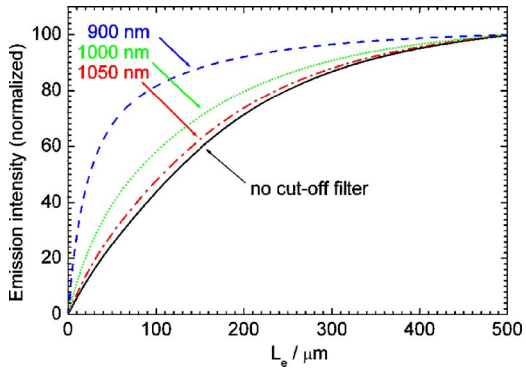

FIG. 3. (Color online) Normalized luminescence emission intensities expected to be registered by a silicon CCD camera equipped with short pass filters with variable cutoff wavelengths of 900 nm (dashed), 1000 nm (dotted), and 1050 nm (dash dotted) as a function of the electron diffusion length in a 300 μm thick silicon solar cell. The bottom curve shows that dependence for a measurement without a short pass filter.

ferent short pass filters; the latter modeled as a step function according to $T_{\text{filter}}=1$ for $\lambda<\lambda_{\text{cutoff}}$ and $T_{\text{filter}}=0$ for $\lambda \geqslant \lambda_{\text{cutoff}}$.

Figure 3 shows the numerically integrated detectable photon currents for short pass filters with cutoff wavelengths ranging from 900 to 1050 nm (a curve calculated for a measurement with no filter is also included). These data are normalized at large diffusion length, i.e., they represent the signals relative to what would be measured with a completely homogeneous carrier concentration; the latter pinned to $n_e(0)$ by the applied voltage according to Eq. (1). Importantly, the variation as a function of the diffusion length of that relative luminescence signal is different for different short pass filters being used. For the 900 nm short pass filter, a strong dependence of the normalized luminescence signal on the diffusion length is predicted for $L_e<50$ μm, and relatively little additional variation for $L_e>100$ μm. This is expected because the additional carriers that diffuse deeper into the cell for longer diffusion lengths do not affect the measured signal at short wavelengths due to reabsorption. In contrast, without a short pass filter, some photons with penetration depths on the order of 300 μm or larger are being measured (see Fig. 2) and, in that case, the variation of the normalized luminescence signal is relatively stronger for long wavelength (bottom curve in Fig. 3). Figure 3 thus shows that the short wavelength part of the luminescence spectrum that is measured with a 900 nm short pass filter selectively gives information about the carrier density near the front surface (i.e., near the junction), while measurements without filter or with a longer wavelength (e.g., 1000 nm) short pass filter are more strongly affected by the carrier density profile throughout the entire device.

Diffusion length from a single luminescence image

The results from Fig. 3 predict a direct relationship between the measured luminescence intensity and the diffusion length, which suggest that, in principle, the diffusion length distribution in a solar cell can be determined by measuring a single EL image, as was proposed and demonstrated experimentally by Fuyuki *et al.*[2] The graph, however, also shows

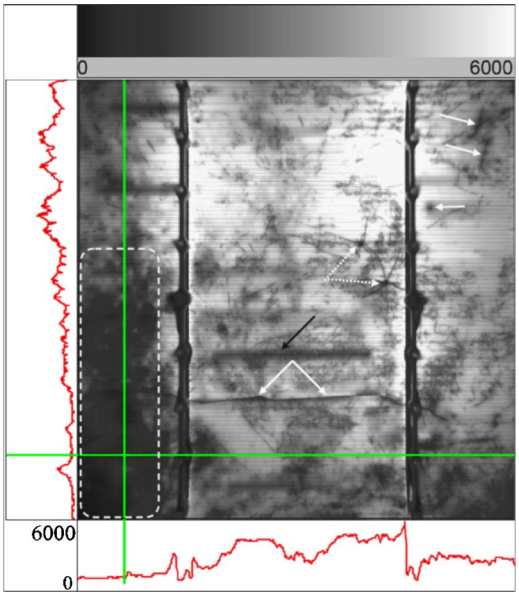

FIG. 4. (Color online) Electroluminescence image of a multicrystalline silicon solar cell with an area of 12.2×12.2 cm^2. The image is taken with a 1000 nm short pass filter and with a data acquisition time of 1 s (see text for details).

that the assumption of Fuyuki *et al.* of the intensity varying linearly with the diffusion length is only valid for small diffusion lengths. In addition, to obtain values for the diffusion length from the luminescence intensity, it is necessary to calibrate the intensity curve in Fig. 3, e.g., by comparison with the intensity of a solar cell, for which the diffusion length is known (e.g., much larger than the cell thickness) and which is in exactly the same geometry (thickness, surface morphology, antireflection coating, voltage, etc.).

Another, far more severe problem with the approach of Fuyuki *et al.* is the effect of lateral voltage variations across the cell. Due to the exponential relationship between the local excess minority carrier density and the voltage [Eq. (1)], a small variation of the voltage of ~60 mV results in a very large variation of the measured luminescence intensity by a factor 10. In EL images taken with a current density equivalent to 1 sun illumination, lateral variations in the voltage on that order can be caused, e.g., by local variations of the series resistance or by broken metal grid fingers.[11]

As an example, Fig. 4 shows an EL image of a 12.2×12.2 cm^2 multicrystalline silicon solar cell measured with a 1000 nm short pass filter mounted in front of the CCD camera. The cell was processed on industrial directionally solidified multicrystalline material using a standard industrial screen-printing process including isotexturing of the surface. A prominent feature in that image is the dark region in the bottom left section of the cell (dashed rectangle), in which the luminescence intensity is up to a factor of 5 lower than the average intensity from that cell. In a PL image taken on the same cell but with the cell operated near the maximum power point (image not shown here), this area appears brighter than the rest of the cell, demonstrating that a locally enhanced series resistance is responsible for the reduced EL intensity from that area[11] and not a reduced diffusion length. This example emphasizes the significant influence of lateral

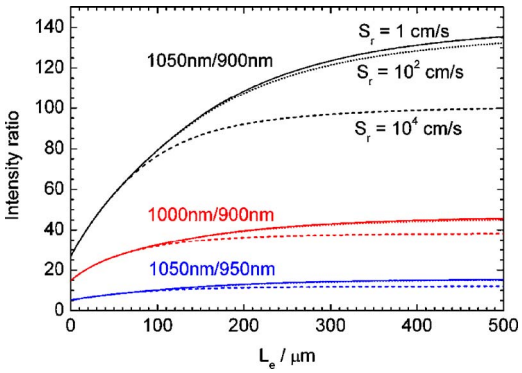

FIG. 5. (Color online) Calculated ratio of electroluminescence intensities, each measured with a different short pass filter. The cutoff wavelengths for the filters are indicated. Results for each signal ratio are shown for three different rear surface recombination velocities S_r=1 cm/s (solid line), 100 cm/s (dotted), and 10^4 cm/s (dashed), respectively.

voltage variations on the luminescence intensity, which is completely ignored in the simplified analysis of a single luminescence image in terms of the diffusion length.[2]

Diffusion length determined from the ratio of two luminescence images

In order to avoid the necessity of a calibration and to eliminate the effect of a laterally inhomogeneous voltage distribution, we propose to measure at least two luminescence images in different wavelength ranges. The latter may be defined by two different short pass filters mounted in front of the camera objective. According to Eqs. (6) and (7), the luminescence signals in different spectral ranges will be affected by variations of the voltage by the same exponential factor. By dividing two luminescence signals, the effect of an inhomogeneous voltage distribution, therefore, cancels out.

Figure 5 shows the theoretical results for the ratio of the expected luminescence signals for various pairs of short pass filters as a function of the diffusion length L_e. The division of two *relative* luminescence signals measured with two different short pass filters gives a number which is indicative of the *absolute* diffusion length and which is free from all external effects that affect the measured intensity, such as the voltage. In Fig. 5, three curves are shown for each combination of filters for rear surface recombination velocities of $S=0$, 100, and 10^4 cm/s. It is seen that the observed ratios of luminescence intensities are little affected for $S<100$ cm/s. In contrast, for $S=10^4$ cm/s, the carrier distribution no longer varies significantly with the diffusion length L_e for $L_e>100$ μm, but is governed by surface recombination. In this case, the analysis of luminescence intensity ratios yields an effective diffusion length instead of the bulk diffusion length, a problem that is known for other methods as well. At least a reasonably accurate estimate of the rear surface recombination velocity is, thus, required to analyze absolute diffusion lengths from intensity ratios. The combinations of filters used for the calculations shown in Fig. 5 are only some possible examples which show a strong enough dependence on the diffusion length. Other combinations would give similar results.

EXPERIMENTS

Two dielectric short pass filters with cutoff wavelengths of 900 and 1000 nm, respectively, were used for this study. Our experiments revealed small nonhomogeneities across the area of both short pass filters being used, resulting in relative lateral signal variations of luminescence images of about 5% upon rotation of the filter by 90°. To reduce the influence of these filter nonhomogeneities, each luminescence image was measured by averaging four otherwise identical exposures, with the filter being rotated by 90° after each exposure. This averaging procedure was employed here in order to avoid the nonideal filter properties limiting the accuracy of the method. While causing longer total data acquisition time, this complication is purely a result of the nonideal filters being used here and does not represent a fundamental requirement or limitation of the method. Further work will focus on identifying more homogeneous dielectric filters.

Figure 4 shows an EL image taken with a silicon CCD camera that was cooled to −30 K and with the 1000 nm short pass filter. A current of 30 mA/cm^2 (similar to the short circuit current of the cell at 1 sun illumination) was fed into the bus bars of the cell via two arrays of ten spring loaded contact pins. The contacting stage available for this study is not ideal, as the spring loaded pins and the rail they are mounted in are partially visible in the luminescence images in the vicinity of the bus bars, thereby shading part of the cell. This is only a practical and temporary limitation of our specific setup.

As discussed above, the dark area on the bottom left hand side of the EL image shown in Fig. 4 (dashed vertical rectangle) is caused by a locally enhanced series resistance. A variety of localized brighter spots are observed within that area near the grid fingers, which indicates relatively lower localized series resistance. Similar observations were recently reported[11] and interpreted as local spots where the front grid makes better contact to the silicon than in the surrounding area of enhanced series resistance. In addition, the image shows the influence of several broken metal grid fingers (e.g., black arrow in Fig. 4) which, as reported previously,[4,12] are characterized by dark lines along the grid finger in EL images. Two cracks on the left side of the right hand bus bar (dotted white arrows) and a large horizontal crack (two white arrows) were introduced during manual cell handling at UNSW. Neither the large horizontal crack nor the two smaller cracks were present during the spectrally resolved LBIC measurement shown below, which was carried out at Fraunhofer ISE, Germany, prior to shipping the cell to UNSW. The three solid white arrows in the top right corner indicate two lengthy and one pointlike area of reduced EL intensity. The blurring of the EL intensity indicates a strong lateral current flow into those areas. However, from this single EL image, it is not possible to determine whether these regions correspond to local shunts or to very active recombination sites.

The features highlighted in the EL image shown in Fig. 4 provide information about various fault mechanisms and electronic defects present in that solar cell. However, these features lead to strong relative variations of the EL intensity

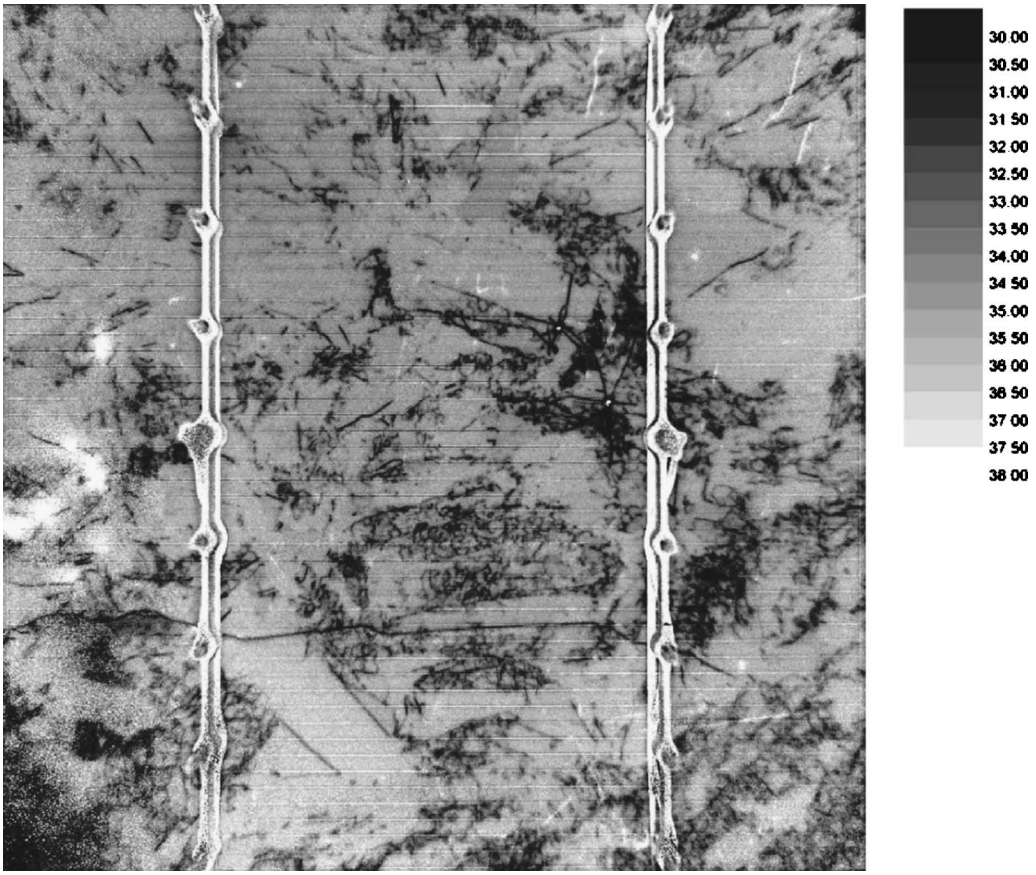

FIG. 6. Intensity ratio of two electroluminescence images taken under identical operating conditions of the solar cell but using two different short pass filters with cutoff wavelengths of 900 and 1000 nm, respectively. The large voltage related intensity variations observed in the individual images (see Fig. 4) are eliminated.

by up to a factor of 5, as seen in the cross sections shown on the left hand side and at the bottom of Fig. 4. The cross sections represent the counts per pixel along the vertical and horizontal lines in Fig. 4, respectively, on a scale from zero to 6000 counts/s. These variations, which are not related to diffusion length variations, make an analysis of this individual image in terms of variations of the diffusion length impossible.

A second luminescence image was measured under identical operating conditions of the solar cell, but with a 900 nm short pass filter replacing the 1000 nm short pass filter. That second image, which is not shown here, exhibits the same features as the image shown in Fig. 4. Figure 6 shows the pixel by pixel ratio of the two EL images taken with the 1000 nm short pass filter and with the 900 nm short pass filter, respectively. The ratio was corrected for the ratio in data acquisition times for the two measurements. The comparison of that ratio image with Fig. 4 shows that most of the voltage related intensity variation observed in the individual images cancels out in the ratio, as predicted theoretically. Even the quite substantial intensity variations in the individual images that are caused by high series resistance, by broken fingers, by cracks, or by significantly higher current flow into the regions near the bus bars are not visible in the intensity ratio image.

The remaining intensity variations in the ratio image from Fig. 6 reveal the variation of the diffusion length L_e. The theoretical curves shown in Fig. 5 were calculated for perfect short pass filters, assuming a step function for their transmission. For the conversion of the experimental luminescence intensity ratio from Fig. 6 into a diffusion length, that theoretical relationship was calculated taking into account the experimentally measured wavelength dependent transmittance of the 900 and 1000 nm short pass filters, respectively, and the wavelength dependent reflectance of the solar cell. Both the transmittance of the filters and the reflectance of the solar cell were measured with a Cary 500 spectrophotometer. The resulting theoretical curve is very similar to the curve in Fig. 5. Because it is specific to the filters used in our experiments, the curve is not shown here.

The diffusion length distribution calculated from the ratio of the two luminescence images (Fig. 6) using this theoretical relationship is shown in Fig. 7. The theoretical relationships between the intensity ratio and the diffusion length (Fig. 5) converge towards constant values for large diffusion length. The white regions that are observed in the ratio image shown in Fig. 6 correspond to intensity ratios that are larger than this saturation value and are, thus, not physically meaningful within the above theoretical model for the carrier distribution. Possible origins for these deviations will be discussed further below. In the conversion of intensity ratios into diffusion length, all areas with intensity ratios greater than 37.5 were converted into a diffusion length greater than 330 μm, which means that in Fig. 7 they are mapped with

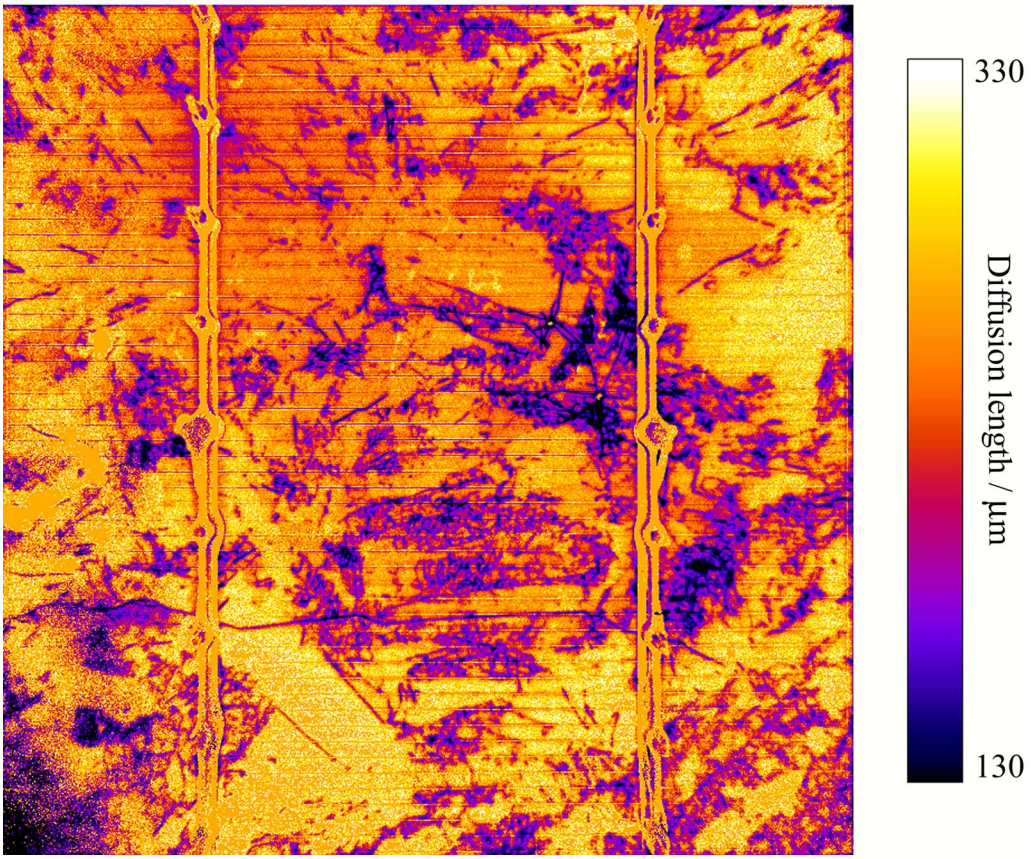

FIG. 7. (Color online) Diffusion length distribution calculated from the intensity ratios from Fig. 6. The color bar gives the diffusion length in micrometers.

the same color. Small diffusion lengths that are observed in the bottom left corner of Fig. 7 result from the very high series resistance effects in that area, which appear to be not perfectly eliminated in the intensity ratio.

For comparison, Fig. 8 shows a map of the diffusion length distribution of the same cell measured with spectrally resolved LBIC. Given that the results from Fig. 7 are obtained from two relative luminescence measurements with very strong lateral features resulting from various fault mechanisms, good quantitative agreement between the two images is observed. The LBIC data span a larger dynamic range with diffusion lengths ranging from $\sim 60\ \mu$m in the low quality areas to greater than 300 μm in the good areas. For comparison, the lowest quality areas in the luminescence image are on the order of 100 μm, with similar values ($\sim 300\ \mu$m) as in the LBIC data for the good areas. In the cell investigated in this study, the areas of low diffusion length are grain boundaries or dislocation networks with fairly small feature sizes. Lateral carrier diffusion from adjacent areas of higher minority carrier diffusion lengths can affect the carrier distribution within these low quality areas, which is currently thought to reduce the contrast between good and bad areas in the luminescence results. For cells with larger areas (e.g., grains) of high and low minority carrier lifetimes, respectively, this smearing effect will be less of a problem.

Transient features

After turning on the forward current through the cell for the EL measurements, we observe an initial gradual increase of the luminescence signal with time, which is not related to temperature effects and not correlated to electrical current variations. With a forward current density equivalent to 1 sun operating conditions, the luminescence signal reached a stable value after 1 min in our experiments. Such observations can be related, e.g., to the breaking of iron-boron pairs[13,14] or to the formation/dissociation of boron-oxygen complexes[15] in the bulk of the cell. A discussion of bias induced degradation in silicon solar cells can be found in Ref. 16. Importantly, such transient effects can strongly impact on the accuracy of our method, which relies on both luminescence measurements being taken under identical operating conditions. Significant changes within the solar cell material during or between the two luminescence measurements influence the intensity ratio and, thereby, the measured diffusion length. A stable luminescence signal must, therefore, be reached first before the two luminescence images are measured. As discussed above, this can mean, in practice, that certain types of cells must be forward biased for some time before the measurements are carried out or that both measurements must be made within a short time interval. The diffusion length that is subsequently calculated from our measurements corresponds to the diffusion length in the saturated state and, as such, is relevant to the solar cell operation, because the solar cell will also normally be operated in that state. As a convenient way to check that transient features have no significant influence on the accuracy of the method, a third luminescence image could be measured that repeats the first measurement with the same filter (the 1000 nm short

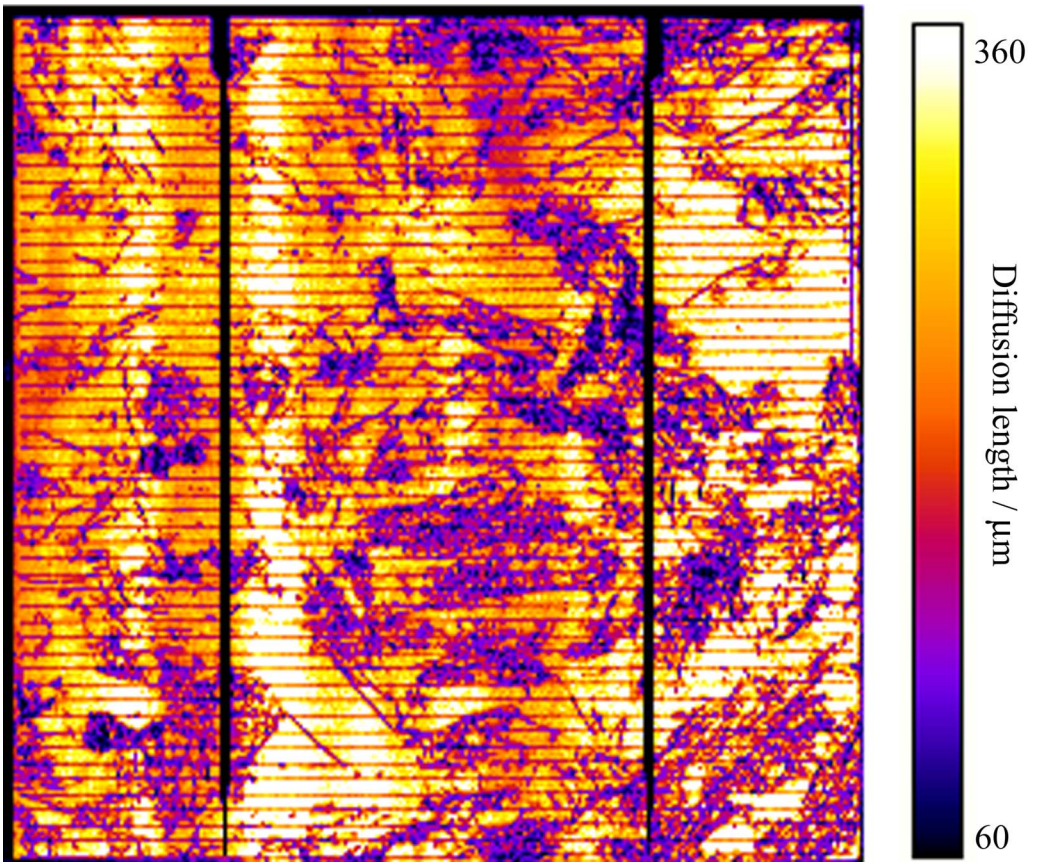

FIG. 8. (Color online) Diffusion length of the solar cell from Fig. 7, determined from a spectral LBIC map.

pass filter in the above example). No significant variation between the first and third images taken should be detectable.

Another unexpected transient feature was observed within the high series resistance area. The white regions with intensity ratios greater than 37, seen on the left hand side of Fig. 6, are caused by blinking of the luminescence intensity in these areas. We observe that, in repetitive measurements of the intensity ratio, these features sometimes appeared as bright spots, sometimes as dark spots, and sometimes they completely disappeared. Our explanation for this effect is an intermittent mechanical and, thus, electrical contact between the metal grid and the silicon, which could be caused, e.g., by thermal expansion upon application of the forward bias.

Injection level dependent diffusion length

In the luminescence based method described here, the two luminescence measurements are carried out under operating conditions that are close to the operating conditions present under 1 sun illumination, i.e., at a well defined injection level. This is of some relevance because the minority carrier lifetime and, thus, the diffusion length can vary by orders of magnitude as a function of the injection level, especially in multicrystalline silicon. In spectral LBIC measurements, the solar cell is operated under external short circuit conditions and under fairly intense local illumination by various modulated laser diodes with different wavelengths. The estimation of the injection level under such experimental conditions is not trivial and depends strongly on the experimental setup and the exact device properties. In LBIC experiments, the minority carrier diffusion length is, thus, determined at an injection level that may not be defined as precisely as in the luminescence method discussed here. Given these considerations, the agreement between the luminescence results and the LBIC map (Figs. 7 and 8, respectively) is surprisingly good.

Sharpening of images

Some features appear significantly sharper in the intensity ratio image from Fig. 6 than in the single EL image from Fig. 4. The features marked with white arrows in the top right corner are a good example. In individual images, the sharpness and, therefore, the ability to localize the defected or shunted region is limited by smearing of the local voltage, which in turn is a series resistance effect caused by lateral currents flowing through the emitter from good quality regions into low quality regions.[6,17,18] As discussed above, the intensity ratio removes any effects caused by lateral voltage variations and, thereby, results in a sharper image allowing a more accurate localization, e.g., of shunted areas.

Shunt detection

The areas indicated by white arrows in Fig. 4 appear as white regions in the intensity ratio shown in Fig. 6. Indeed, the ratio is greater than 38 in those areas and, thus, larger than theoretically predicted for an infinite diffusion length. In order to explain this observation, we note that in the above

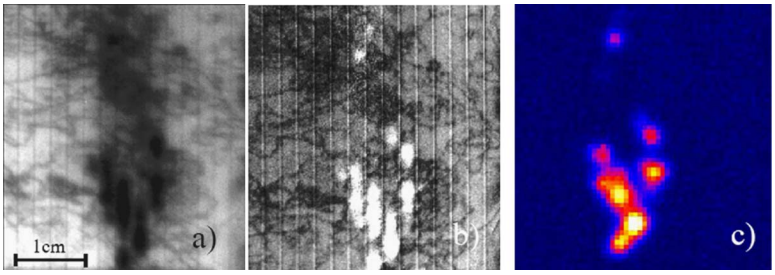

FIG. 9. (Color online) (a) Electroluminescence intensity from a 3.2×3.2 cm^2 section of a shunted multicrystalline silicon cell measured with a 1050 nm short pass filter. (b) Ratio of EL intensities measured with a 1050 nm short pass filter and with a 900 nm short pass filter, respectively. (c) Dark lock-in thermography (Ref. 19) measurement carried out with 0.5 V reverse bias.

theoretical model the carrier concentration always decays with increasing distance from the junction. There are, however, cases where the distribution of carriers from the surface into the interior of a solar cell does not follow Eq. (4). Specifically, there are cases where the carrier density near the junction is lower than in the bulk. One example is the presence of a localized shunt in the *p-n* junction, which causes the voltage and, thereby, the minority carrier concentration at the junction to be reduced. The shunted region will, therefore, emit less luminescence and appear as a dark spot in a single CCD image (white arrows in Fig. 4), particularly at short wavelengths at which the carrier concentration close to the *p-n* junction is probed. If the shunt has a small lateral extension and if it is not going through the whole thickness, lateral bulk minority carrier diffusion will result in a relatively higher carrier concentration further away from the junction and, thereby, in a relatively higher long wavelength emission. In the ratio of two images taken at long and short wavelengths, respectively, the shunt will, therefore, appear particularly bright, with intensity ratios even exceeding the ratios expected for an infinitely large diffusion length (homogeneous profile). Thus, a dark spot in a single image which turns bright in the ratio image may be identified as a shunt. Dark lock-in thermography[19] (DLIT) measurements with 0.5 V applied voltage in forward and reverse directions were carried out and revealed no shunt type behavior in the areas indicated by white arrows in Fig. 6. We, therefore, conclude that the high luminescence intensity ratios in those areas are caused by recombination active defects at the surface, caused, e.g., by scratches, which have a similar influence on the relative carrier profile as shunts.

In order to demonstrate the possibility of distinguishing shunted regions from bulk defects, we investigated a shunted industrial multicrystalline silicon solar cell with an efficiency of 14.0% (compared to around 15% typical for nonshunted cells from the same batch) and with an area of 15×15 cm^2. A shunt resistance of 1.33 Ω was determined for that cell from the reverse current at a reverse bias of −3 V. A DLIT measurement on that cell revealed localized shunts within a 3.2×3.2 cm^2 area near one of the bus bars [Fig. 9(c)]. Figure 9(a) shows an EL image of that section taken with a 1050 nm short pass filter, and Fig. 9(b) shows the intensity ratio of two EL images taken with a 1050 nm short pass filter and with a 900 nm short pass filter, respectively. The intensity ratio in the shunted region takes on values up to ~300, which is more than three times more than the ratio in the nonshunted region, where it varies between 70 and 100. The comparison of Figs. 9(a)–9(c) shows that, in cells with moderate to strong local shunts, the intensity ratio image allows identifying shunted regions and clearly distinguishing them from bulk recombination active regions in the vicinity.

CONCLUSIONS

A quantitative determination of the spatially resolved diffusion length from the ratio of two luminescence images measured with two different spectral filters has been discussed theoretically and demonstrated experimentally on a screen printed multicrystalline silicon solar cell. Good agreement is observed between the absolute diffusion length from that method and the results from a spectrally resolved LBIC map.

In this study, we used a silicon CCD camera with a resolution of 1024×1024 pixels. Although a silicon CCD is much less sensitive to the long wavelength luminescence emission of a silicon solar cell than to visible radiation (only picking up about 3%–5% of the total emitted luminescence even without a filter), taking an image with short pass filtering requires only about 1 s for $\lambda_{cutoff}=1000$ nm and about 100 s for $\lambda_{cutoff}=900$ nm. Allowing for 1 min of forward biasing of the cell prior to the luminescence measurements, a high resolution map of the diffusion length can, thus, be obtained in under 3 min, much faster than the measurement time for a LBIC map with lower spatial resolution. The data acquisition time can be further reduced by binning of pixels, thereby sacrificing spatial resolution. Binning 5×5 pixels still yields a diffusion length image with 204×204 pixels and can be achieved with a total exposure time of only 4 s. In cases where no transient effects are observed, a diffusion length image can, thus, be taken in a matter of a few seconds.

The variation of the luminescence intensity ratio with diffusion length (Fig. 5) is weak and also depends more strongly on the surface recombination velocity for large diffusion lengths. As a result, the luminescence technique discussed here becomes less quantitative for diffusion lengths that are comparable to or larger than the thickness of the cell, similar to LBIC measurements. Our results indicate that in small areas of reduced minority carrier diffusion length that have a lateral extension on the order of the diffusion length, a quantitative analysis of the luminescence intensity ratio can overestimate the diffusion length. In contrast, our method gives reliable values for larger regions of constant diffusion length. Surface texturing leads to comparable errors in the luminescence technique and in LBIC, because the texture affects the angle between the solar cell surface and the internal light path (for incident light in LBIC and for emitted light in luminescence). For geometrical surface textures like inverted pyramids, the angle of the internal light path is pre-

dictable and can be accounted for analytically. For random textures, it may be necessary to empirically determine correction factors to determine absolute diffusion lengths. The latter statement again holds equally for both the luminescence technique and for LBIC.

The method that has been presented here is not limited to electroluminescence, but with some modifications, it can also be applied to photoluminescence. Photoluminescence imaging[7] has the great advantage that it can be applied to silicon wafers at all stages of solar cell production, from raw wafers through to finished solar cells. The methods described here could, thus, become a useful tool in calibrating photoluminescence images on silicon wafers; the latter generally not a trivial task due to the dependence of the luminescence signal on the minority carrier lifetime, the doping concentration, the sensitivity of the detector, and the optical properties of the sample and the incident intensity. In previous work on PL imaging, a powerful infrared laser was used for excitation, leading to a depth dependent generation profile that extends into the cell and is difficult to describe by the theoretical model above. In that case, in order to determine the theoretical relationship between the luminescence intensity ratio and the diffusion length, carrier density profiles for different diffusion lengths may be calculated numerically, e.g., using PC1D simulations.[20]

A quantitative analysis of a single electroluminescence image in terms of absolute local diffusion length variations as proposed by Fuyuki *et al.*[2] is possible in principle, but is, however, limited in practice to very specific cases where lateral variations of the voltage can be neglected. Even small voltage variations of 10 mV will lead to large relative errors in the resulting diffusion length of $\sim 50\%$. As has been shown here, such errors resulting from lateral voltage variations are eliminated by calculating the ratio of two luminescence images measured in different spectral ranges but with identical operating condition of the solar cell. As further advantages of the method proposed here, photon reabsorption within the silicon sample is accounted for quantitatively and images of the absolute diffusion length are obtained without the need for calibration.

ACKNOWLEDGMENTS

The authors would like to thank Martin A. Green from UNSW for valuable discussions and also Martin Kasemann from Fraunhofer Institute for Solar Energy Systems, Freiburg, Germany, and Jan Bauer from Max Planck Institute for Microstructure Physics, Halle, Germany, for carrying out lock-in thermography measurements. The supply of a shunted screen-printed solar cell by Hans-Peter Hartmann, Deutsche Cell GmbH, Freiberg, Germany, is also gratefully acknowledged. The Centre of Excellence for Advanced Silicon Photovoltaics and Photonics is supported under the Australian Research Council's Centres of Excellence Scheme.

[1] W. Warta, J. Sutter, B. Wagner, and R. Schindler, Proceedings of the Second World Conference on Photovoltaic Energy Conversion, Vienna, Austria, 1998, p. 1650.
[2] T. Fuyuki, H. Kondo, T. Yamazaki, Y. Takahashi, and Y. Uraoka, Appl. Phys. Lett. **86**, 262108 (2005).
[3] T. Fuyuki, H. Kondo, Y. Kaji, T. Yamazaki, Y. Takahashi, and Y. Uraoka, Proceedings of the 31st IEEE Photovoltaic Specialists Conference, Orlando, 2005, p. 1343.
[4] T. Trupke, R. A. Bardos, M. D. Abbott, F. W. Chen, J. E. Cotter, and A. Lorenz, Proceedings of the WCPEC-4, Waikoloa, 2006, p. 928.
[5] K. Bothe, P. Pohl, J. Schmidt, T. Weber, P. P. Altermatt, B. Fischer, and R. Brendel, Proceedings of the 21st European Photovoltaic Solar Energy Conference, Dresden, Germany, 2006, p. 597.
[6] M. Kasemann, M. C. Schubert, M. The, M. Köber, M. Hermle, and W. Warta, Appl. Phys. Lett. **89**, 224102 (2006).
[7] T. Trupke, R. A. Bardos, M. C. Schubert, and W. Warta, Appl. Phys. Lett. **89**, 044107 (2006).
[8] P. Würfel, S. Finkbeiner, and E. Daub, Appl. Phys. A: Mater. Sci. Process. **A60**, 67 (1995).
[9] P. Würfel, *Physics of Solar Cells* (Wiley-VCH, Weinheim, 2005).
[10] H. A. Weakliem and D. Redfield, J. Appl. Phys. **50**, 1491 (1979).
[11] T. Trupke, E. Pink, R. A. Bardos, and M. D. Abbott, Appl. Phys. Lett. **90**, 093506 (2007).
[12] Y. Takahashi, Y. Kaji, O. Ogane, Y. Uruoka, and T. Fuyuki, Proceedings of the WCPEC-4, Hawaii, 2006, p. 924.
[13] G. Zoth and V. Bergholz, J. Appl. Phys. **67**, 6764 (1990).
[14] J. Schmidt, Prog. Photovoltaics **13**, 325 (2005).
[15] J. Schmidt and K. Bothe, Phys. Rev. B **69**, 024107 (2004).
[16] S. W. Glunz, E. Schäffer, S. Rein, K. Bothe, and J. Schmidt, Proceedings of the WCPEC-3, Osaka, Japan, 2003, p. 919.
[17] J. C. Goldschmidt, O. Schultz, and S. W. Glunz, Proceedings of the 20th EPVSC, Barcelona, Spain, 2005, p. 663.
[18] T. Trupke, R. A. Bardos, M. D. Abbott, K. Fisher, J. Bauer, and O. Breitenstein, Proceedings of the International Workshop on Science and Technology of Crystalline Silicon Solar Cells, Sendai, Japan, 2–3 October 2006 (unpublished).
[19] O. Breitenstein and M. Langenkamp, *Lock-In Thermography: Basics and Use for Functional Diagnostics of Electronic Components* (Springer, Heidelberg, 2003).
[20] P. A. Basore and D. A. Clugston, Proceedings of the 25th IEEE Photovoltaic Specialists Conference 1996, p. 377.